

Condensed Matter and Interphases (Kondensirovannye sredy i mezhfaznye granitsy)

Original articles

DOI: <https://doi.org/10.17308/kcmf.2020.22/2534>

eISSN 2687-0711

Received 02 February 2020

Accepted 15 February 2020

Published online 25 March 2020

Phase Equilibria in the Sn–As–Sb System with Tin Concentrations of Less than 50 mol%

© 2019 T. P. Sushkova[✉], G. V. Semenova, A. V. Sheveljukhina, S. V. Kannykin, E. Yu. Proskurina, A. V. Nerushev

Voronezh State University 1 Universitetskaya pl., Voronezh 394018, Russian Federation

Abstract

Tin- and antimony-based alloys, including SnSb and other compounds of the $A^{IV}B^V$ type, are used for the production of anodes for Li^+ - and Na^+ ion batteries. Multicomponent solid solutions allow varying the properties of the material and improve the technical characteristics of the anodes. There is very little information in the literature about solid phase solubility in the Sn–As–Sb system, and the phase diagram of the system has not been studied yet. The aim of this paper was to study the polythermal sections SnAs–Sb and SnAs–SnSb using the X-ray diffraction analysis (XRD) and differential thermal analysis (DTA), as well as to construct a phase equilibria scheme for the Sn–As–Sb system with the range of tin concentrations of less than 50 mol%.

The alloys of the polythermal sections SnAs–Sb and SnAs–SnSb were obtained from pre-synthesized binary compounds and then subjected to homogenizing annealing. The obtained powdered samples were then investigated using differential thermal analysis (DTA) and X-ray diffraction analysis (XRD).

The XRD results showed that all the studied alloys were heterophase mixtures of solid solutions (SnAs), (SnSb) and α' , where α' is a solid solution of tin in the $\text{As}_{1-x}\text{Sb}_x$ phase. The concentration range of solid solutions based on binary compounds at room temperature was below 10 mol %. The DTA demonstrated that in several alloys of the two sections the first endothermic effect was observed at the same temperature (393 ± 2 °C). This temperature corresponds to the peritectic process involving the above-mentioned phases: $L + \alpha' \leftrightarrow (\text{SnAs}) + (\text{SnSb})$.

Using the DTA method and the XRD data, T - x diagrams of polythermal sections SnAs–Sb and SnAs–SnSb were constructed. The coordinates of the invariant peritectic equilibrium $L + \alpha' \leftrightarrow (\text{SnAs}) + (\text{SnSb})$ were determined; a scheme of phase equilibria in the Sn–As–Sb system with the range of tin concentrations of less than 50 mol % was proposed. To construct a complete scheme of phase equilibria in the ternary system, it is necessary to further investigate the SnAs– Sn_4Sb_3 and Sn_4As_3 – Sn_4Sb_3 sections.

Keywords: Sn–As–Sb system, solid solutions, phase equilibria.

For citation: Sushkova T. P., Semenova G. V., Sheveljukhina A. V., Kannykin S. V., Proskurina E. Yu., Nerushev A. V. Phase equilibria in the system Sn–As–Sb with tin concentrations of less than 50 mol%. *Kondensirovannye sredy i mezhfaznye granitsy = Condensed Matter and Interphases*. 2020; 22(1): 106–115. DOI: <https://doi.org/10.17308/kcmf.2020.22/2534>

1. Introduction

The latest technological advancements stimulate the research and development of new high-energy, reliable, and long lifespan devices for energy conversion and storage. Owing to their natural abundance, low cost, and environmental benignity, sodium- and potassium-ion batteries are a promising alternative to commonly used lithium-ion batteries [1–3]. However, the low

energy density and poor life cycle stability limit their commercial applications [2, 4]. The development of high-performance electrode materials is one of the key issues in the production of next-generation alkali-ion batteries.

Anodes based on alloys including Si, Ge, Sn, P, As, Sb, and Bi, have been actively investigated over the past few years [2, 4–22]. The intermetallic compound SnSb is one of the best materials for the production of anodes for Li^+ -ion batteries and is a

✉ Tatiana P. Sushkova, e-mail: sushtp@yandex.ru



The content is available under Creative Commons Attribution 4.0 License.

promising material for the production of Na⁺-ion batteries [4–10]. There are two reasons for this. First, SnSb contains two elements active toward Li. Hence, the uptake and release of lithium ions occurs in the presence of two lithium phases. The formation of a more stable compound of lithium and antimony Li₃Sb results in an increase in volume, which is buffered by the ductile phase of tin. This prevents any significant alterations in the volume that may lead to the decomposition of the anode material [5–7]. Second, the SnSb phase has a layered crystalline structure (rhombohedral lattice, space group R-3m) [23, 24], which allows for easy intercalation of ions of alkali metals into the interlayer space.

Some other compounds of type A^{IV}B^V also have layered structures [25–27], and were tested as anode materials and intercalates [11–22, 28]. For instance, tin phosphide Sn₄P₃ has the same crystal lattice [26] as SnSb, and is one of the best anode materials for Li⁺- and Na⁺-ion batteries [11–16].

One of the ways to enhance the technical characteristics of anodes is to increase the number of elements in the system and to use solid solutions based on pure compounds, rather than the compounds themselves. Modifying the composition of a solid solution we can significantly extend the functional characteristics of the material. This means that it is important to analyse the nature of phase equilibria in multicomponent systems. It was determined that a continuous series of solid solutions Sn₄P₃–Sn₄As₃ and substitutional bounded solid solutions based on SnAs and SnP₃ [29–32] is formed in the system Sn–As–P. Taking into account that Sn₄P₃, Sn₄As₃, Sn₄Sb₃ and SnSb have identical crystal lattices [24–26], while phosphorus, arsenic, and antimony are electronic analogues, and the atoms of As and Sb are close in size (the system As–Sb demonstrates complete miscibility [33]), we can expect the formation of ternary solid solutions in the system Sn–As–Sb as well.

To date the phase diagram of this system has not been well studied. [34] mentions that the earliest study, published in 1919, suggested the possibility of existence of a ternary chemical compound, but its crystalline structure was not determined; later studies did not confirm this suggestion but indicated high miscibility of rhombohedral SnSb and cubic SnAs. It is therefore

important to study the phase equilibria in the ternary system Sn–As–Sb.

The binary systems limiting the ternary system Sn–As–Sb, contain four chemical compounds. Arsenide Sn₄As₃ decomposes peritectically, while SnAs melts congruently [35]. The composition and structure of the two intermediate phases of the system Sn–Sb still cause a lot of controversy. All the previously published versions of the phase diagram of Sn–Sb are thoroughly analysed in [23]. In this study, we used the phase diagram described in [24], which is based on a rigorously conducted experiment using a set of modern research methods. According to [24], SnSb and Sn₄Sb₃ have incongruently melting phases with wide homogeneity regions. Therefore, none of the sections of the studied ternary system can be quasi-binary.

The aim of this paper was to study the polythermal sections SnAs–Sb and SnAs–SnSb using X-ray phase analysis (XRD) and differential thermal analysis (DTA) and to construct a phase equilibria scheme for the Sn–As–Sb system with the range of tin concentrations of less than 50 mol%.

2. Experimental

The alloys whose compositions correspond to the polythermal sections SnAs–Sb and SnAs–SnSb were obtained in two stages. The binary phases were preliminary obtained by means of direct melting of simple chemical substances: Sn-5N tin (99.999 %), As-5N arsenic (99.9997 %), and Sb-000 antimony (99.99%). Arsenic was preliminary purified from oxides by vacuum sublimation. The samples were weighed using electronic scales AR2140 (measurement error ±1·10⁻³ g). The alloys were synthesized in quartz ampoules vacuumed to the residual pressure of 5·10⁻⁴ hPa. The three-component samples underwent homogenizing annealing at 300 °C for 150 hours. The samples were then cooled in the furnace.

X-ray phase analysis was performed using an ARLX'TRA diffractometer with Bragg–Brentano Θ–Θ focusing geometry. The source of radiation was an X-ray tube with a copper anode which had the following characteristics: maximum capacity – 2200 W; λ(Cu-K_{α1}) = 0.1541 nm; λ(Cu-K_{α2}) = 0.1544 nm. The X-ray patterns were

made with a step size of 0.04° and a counting time of 3 seconds per step. The error for determining the interplanar distances d_{hkl} was below $5 \cdot 10^{-4}$ nm. The obtained patterns were interpreted using the Powder Diffraction File of the International Centre for Diffraction Data (ICDD PDF-2, 2012).

Differential thermal analysis (DTA) was performed using a furnace with a programmed heating rate of 5 deg./min and chromel-alumel thermocouples. The signal received from the thermocouples was digitized and processed by the MasterSCADA software package. The reference sample was calcined aluminium oxide placed in a Stepanov quartz vacuumed vessel of approximately the same size as the quartz ampoules containing the studied substances.

The calibration benchmarks for the system were pure substances: tin (232.1 °C), tellurium (449.7 °C), and antimony (630.9 °C) [36]. The error for temperature measurement was below $\pm 2^\circ$. Since the alloys of the studied system have a tendency to undercool, the temperature of phase transformations was determined by the heating curves.

3. Results and discussion

Fig. 1 demonstrates X-ray powder diffraction patterns of certain alloys of the polythermal section SnAs–Sb. When the concentrations of antimony in the samples are low, the diffractograms show peaks attributable to three phases: solid solutions based on tin monosulfide (SnAs) and antimony monosulfide (SnSb), and

tin solid solution in the phase $As_{1-x}Sb_x$ (α'). Since the alloy containing 10 mol% of Sb was not single-phase (Fig. 1a), we can conclude that the concentration range of the SnAs-based solid solution along the section SnAs–Sb at room temperature is below 10 mol%.

The peak shift occurring due to the alteration of the alloy compositions indicates the formation of a SnAs-based solid solution. It is even better demonstrated by the increase in the interplanar distances and the cubic lattice parameter (Table 1). The samples with antimony concentrations of less than 50 % demonstrated few (SnAs) peaks which were of very low intensity, since (SnAs) is formed in these alloys only during secondary or tertiary crystallization and in very small quantities.

The lines corresponding to the solid solution (SnSb) and shifted toward greater angles as a result of substitution of antimony atoms with smaller arsenic atoms, were observed in the X-ray powder diffraction patterns of all the samples.

For all the samples, the 100% intensity line corresponded to the solid solution α' . The number of peaks of this phase increased with higher concentrations of antimony in the alloys. A significant shift of the lines following the alteration of the composition of the samples indicated a significant difference in the composition of this phase. This resulted from the change in the direction of the connodes connecting the melting point and the composition of the crystallised α' -phase.

Table 1. Interplanar distances (d , nm) and the lattice parameter (a , nm) of the SnAs-based solid solution present in the alloys of the section SnAs–Sb

SnAs		The composition (mol. f. Sb) of the alloys of the section SnAs–Sb				
hkl	d	0.10	0.20	0.30	0.40	0.50
111	0.3306	0.3308				
200	0.2862	0.2869				
220	0.2024	0.2042	0.2054	0.2045	0.2045	
311	0.1726	0.1730	0.1749	0.1752		
222	0.1652	0.1655		0.1686		
400	0.1431	0.1433	0.1470		0.1473	0.1474
331	0.1312	0.1319	0.1332	0.1332	0.1332	0.1349
420	0.1280	0.1281		0.1299		
422	0.1168	0.1170	0.1198	0.1198	0.1196	
511	0.1101	0.1102	0.1113	0.1134		
Lattice parameter, a	0.5725	0.5735	0.5799	0.5824	0.5900	0.5977

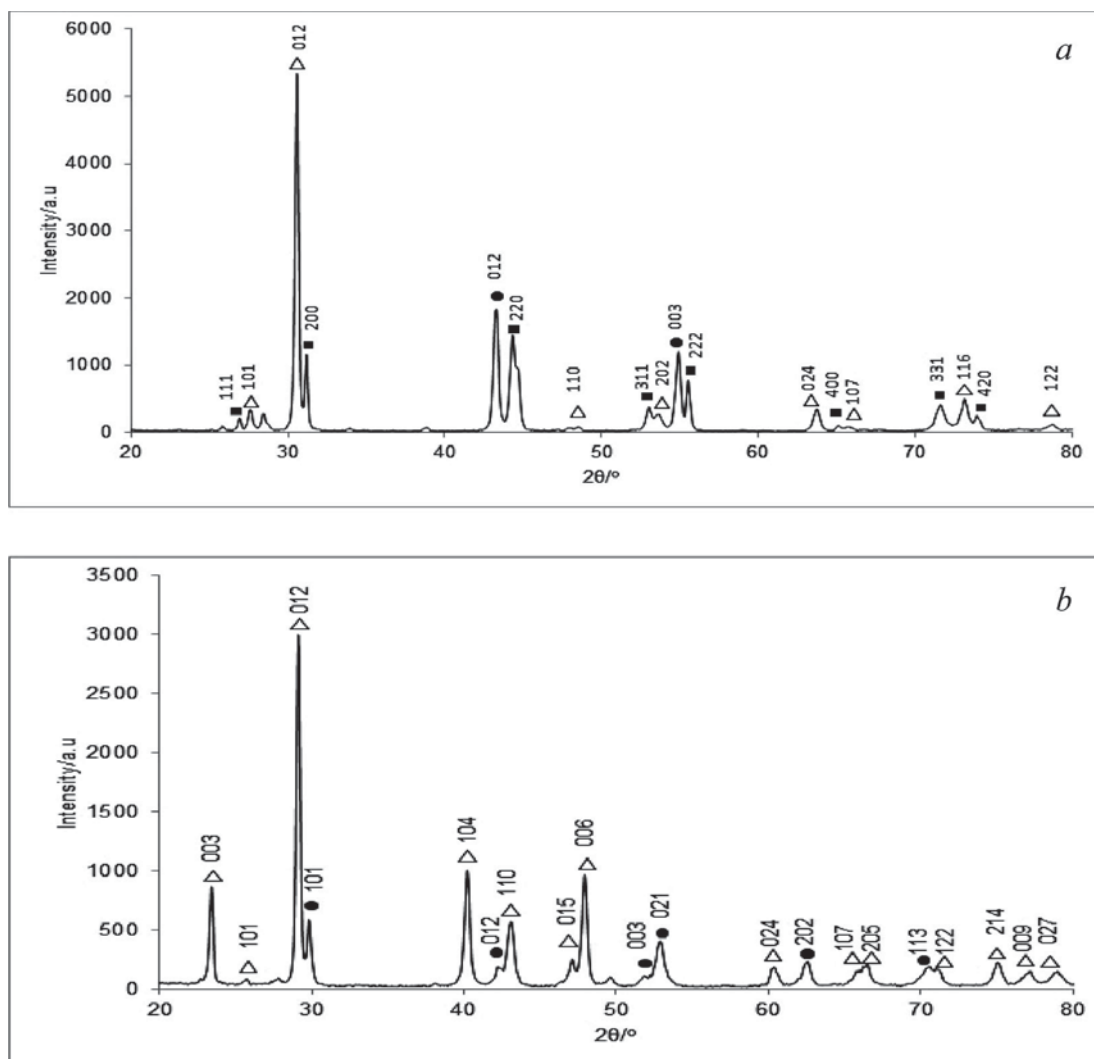


Fig. 1. X-ray powder diffraction patterns of the polythermal section SnAs–Sb: a – 0.10, b – 0.70 mol.f. Sb. Designations: ● – (SnSb), ■ – (SnAs), Δ – α'

The study of the second polythermal section SnAs–SnSb by means of XRD analysis demonstrated that the samples also contained three solid solutions: (SnAs), (SnSb), and α' (Fig. 2). (SnAs) peaks were dominant in the samples with less than 20 mol% of SnSb (Fig. 2a). Then their number and intensity decreased, and the most intense lines corresponded to the solid solution (SnSb) (Fig. 2b). Table 2 presents the calculations of the lattice parameters of the solid solution based on tin monosulfide. It is impossible to evaluate the composition of the solid solution using Vegard's law, since SnAs and SnSb have crystal lattices of different types.

The peaks of phase α' are present in the X-ray powder diffraction patterns of all the samples, but their number and intensity are relatively small. Judging by the absence of single-phase alloys, we

can conclude that the solid phase solubility along the section SnAs–SnSb at room temperature is below 5 mol%.

Differential thermal analysis demonstrated that in several samples of the studied sections the first endothermic effect was observed at nearly the same temperature of 393 ± 2 °C (Fig. 3). In order to interpret the experimental results of the DTA correctly and construct T - x diagrams of the sections, we analysed the crystallization processes of the alloys.

Fig. 4 shows the representation of the T - x - y diagram of the ternary system limited by binary systems. The polythermal section SnAs–Sb intersects the fields of primary crystallization of the SnAs-based solid solution and the solid solution α' . For the alloys whose compositions correspond to the ab segment,

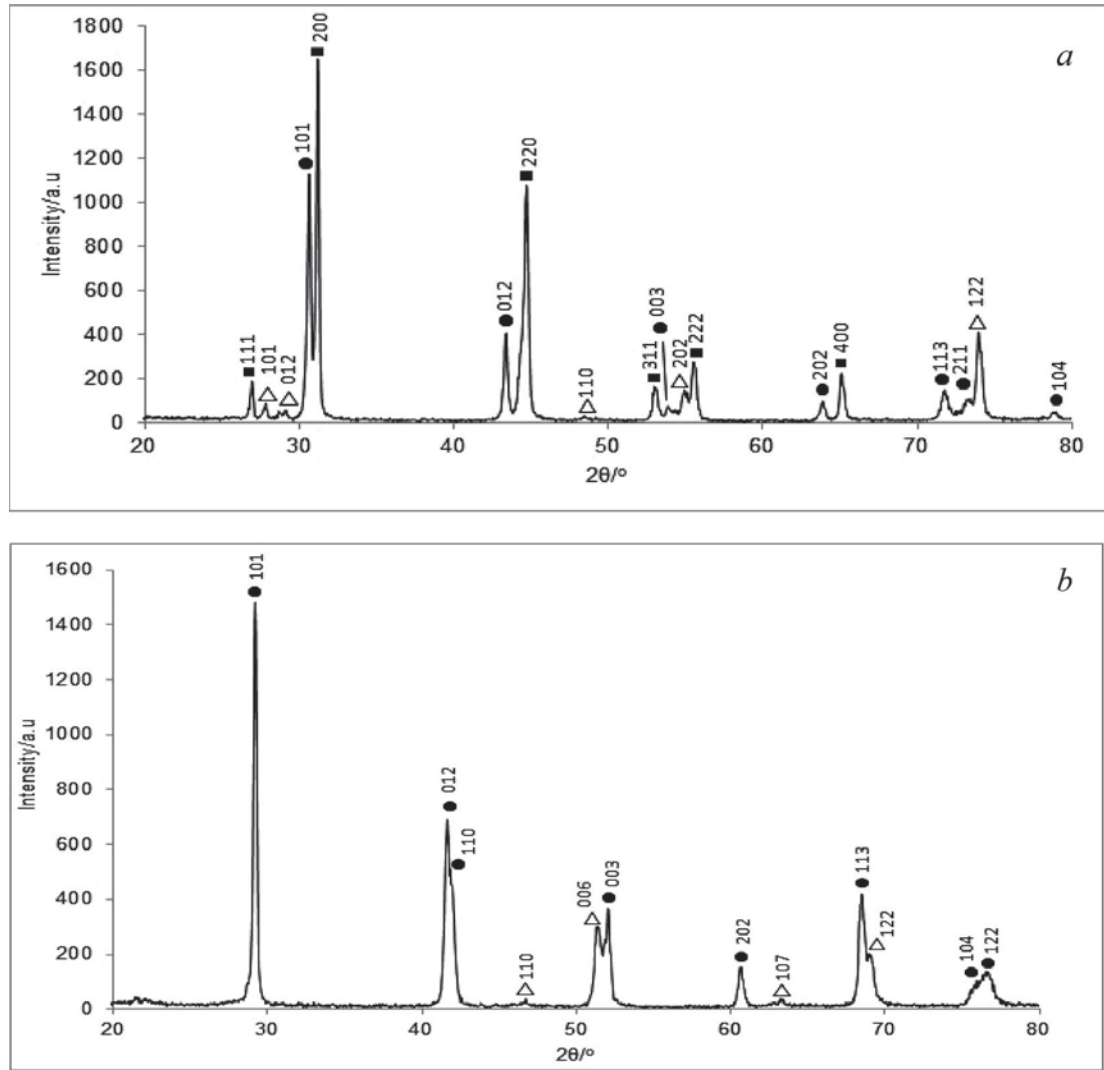


Fig. 2. X-ray powder diffraction patterns of the polythermal section SnAs–SnSb: a – 0.05; b – 0.90 mol.f. SnSb. Designations: ● – (SnSb), ■ – (SnAs), Δ – α'

Table 2. Interplanar distances (d , Å) and the lattice parameter (a , Å) of the SnAs-based solid solution present in the alloys of the section SnAs–SnSb

SnAs		The composition (mol. f. SnSb) of the alloys of the section SnAs – SnSb					
hkl	d	0.05	0.10	0.20	0.30	0.40	0.60
111	0.3306	0.3306	0.3306				
200	0.2862	0.2865	0.2866	0.2876			
220	0.2024	0.2026	0.2029	0.2028	0.2040	0.2043	
311	0.1726	0.1728		0.1729	0.1740	0.1753	0.1758
222	0.1652	0.1654	0.1654			0.1680	0.1687
400	0.1431	0.1433	0.1434	0.1437	0.1437	0.1439	
331	0.1313	0.1316	0.1317				
Lattice parameter, a	0.5725	0.5730	0.5732	0.5742	0.5780	0.5829	0.5909

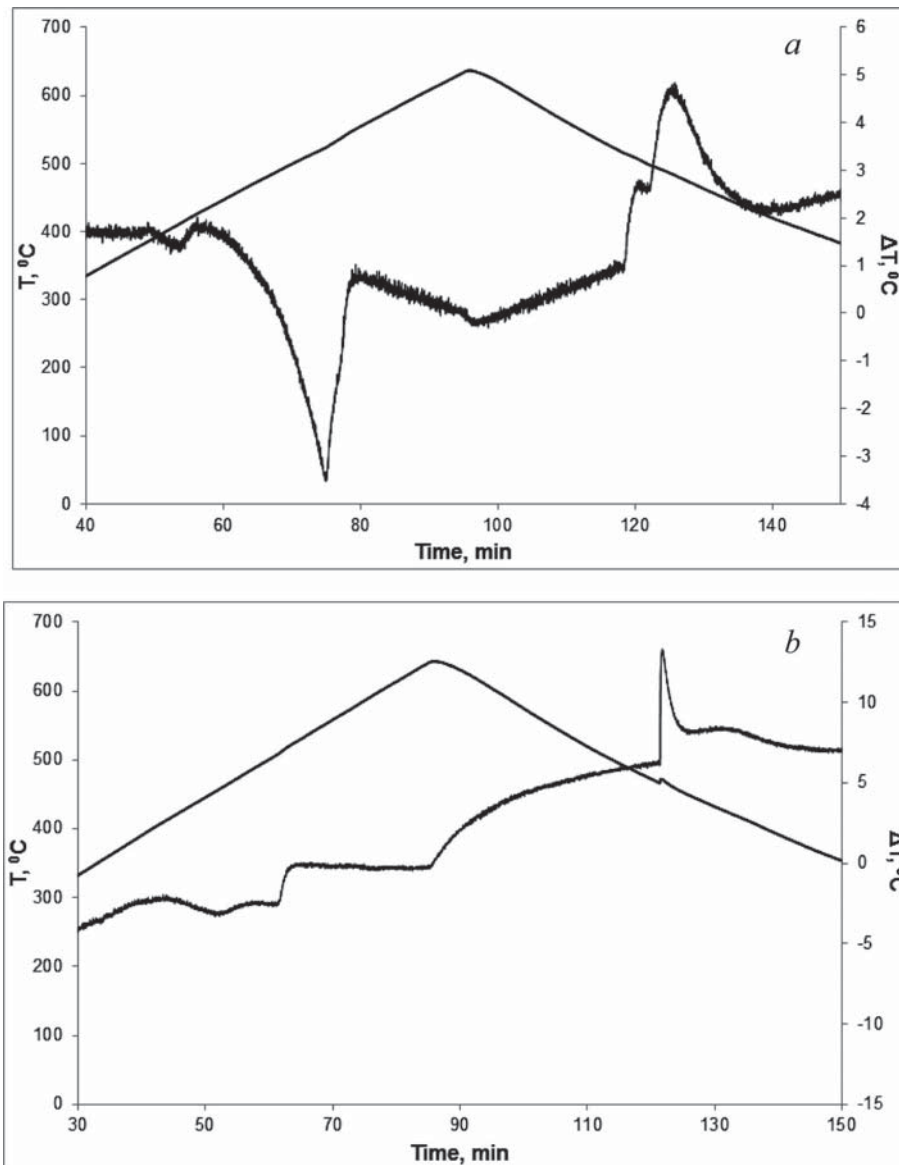


Fig. 3. Thermograms of alloys $(\text{SnAs})_{0.6}\text{Sb}_{0.4}$ (a) and $(\text{SnAs})_{0.4}(\text{SnSb})_{0.6}$ (b)

primary crystallization is carried out according to the $L \leftrightarrow (\text{SnAs})$ scheme; secondary crystallization corresponds to line e_1U_1 ($L \leftrightarrow (\text{SnAs}) + \alpha'$); the process ends at U_1 . For the alloys whose compositions correspond to the bc segment, primary crystallization occurs in the solid solution α' (its composition is different for different alloys); then the figurative melting point falls either on the curve e_1U_1 , or the curve p_2U_1 , along which the peritectic process $L + \alpha' \leftrightarrow (\text{SnSb})$ occurs. For one of the compositions, secondary crystallization does not occur, and the figurative point falls directly on U_1 .

Thus, for all the alloys of the section SnAs–Sb the crystallization process ends at U_1 , which

lies outside the trapezium As–SnAs–SnSb–Sb. It is at this point that the temperature is 393 ± 2 °C, which allows for the peritectic transformation $L + \alpha' \leftrightarrow (\text{SnAs}) + (\text{SnSb})$. On the T - x diagrams of the polythermal sections (Fig. 5) U_1 corresponds to the horizontal, below which there are only solid phases.

The polythermal section SnAs–SnSb also intersects the fields of primary crystallization of solid solutions (SnAs) and α' . The sequence of the crystallization processes of the alloys whose compositions correspond to segments ad and df is the same as that of the alloys corresponding respectively to segments ab and bc on the section SnAs–Sb. The T - x diagram of the section SnAs–

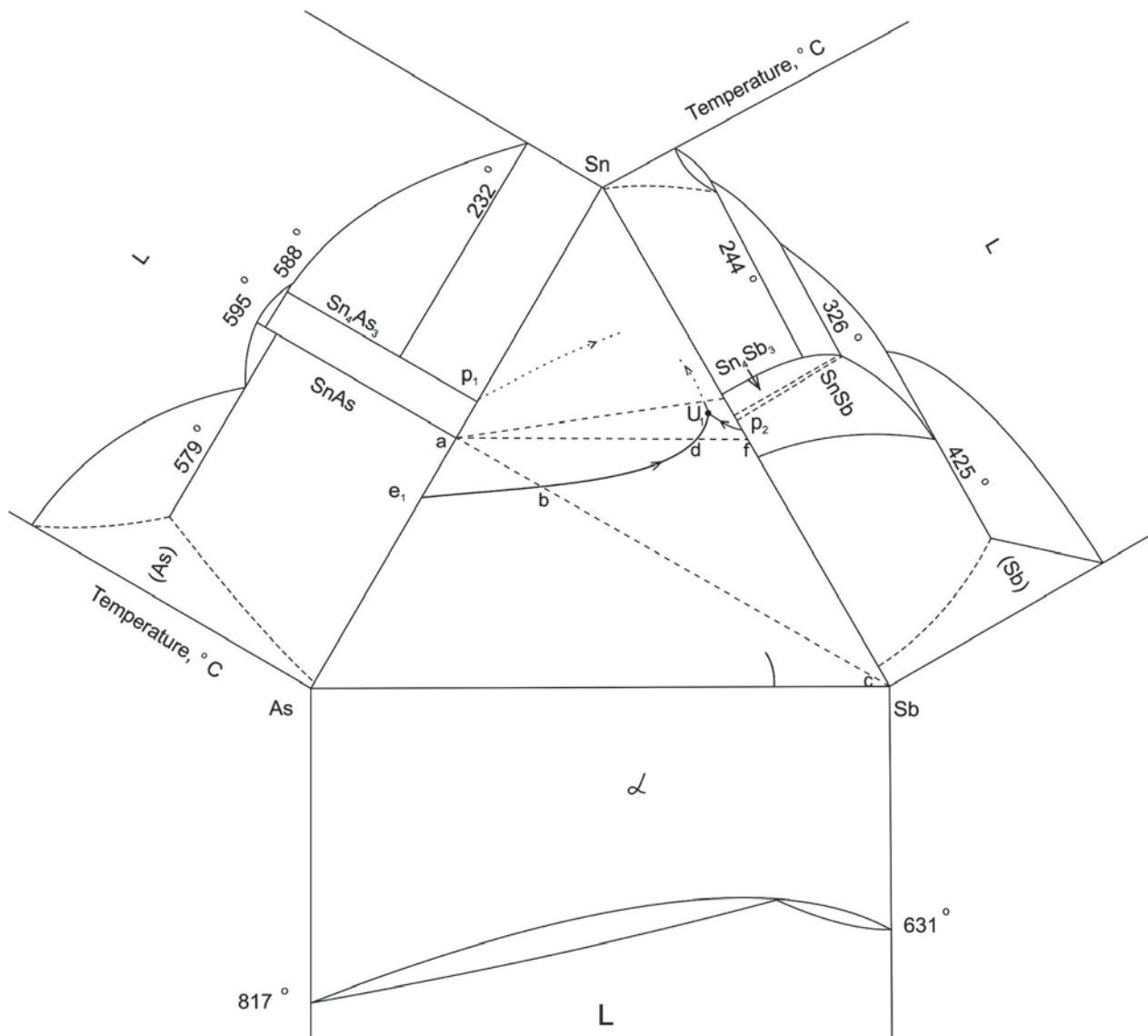


Fig. 4. Scheme of phase equilibria in the Sn–As–Sb ternary system

SnSb is shown in Fig. 5b. The second horizontal at the temperature of 408 ± 2 °C is accounted for by the fact that after primary crystallization of (SnAs) the figurative melting point falls at the same point (*d*) on the monovariant curve e_1U_1 , and secondary crystallization of several alloys begins at the same temperature.

The triple points on *T*-*x* diagrams of the sections (Fig. 5b) correspond to points *b* and *d* on the curve e_1U_1 (Fig. 4). Thus, the results of the DTA allow to determine the coordinates of the monovariant equilibrium line e_1U_1 . This curve intersects the section SnAs–Sb at the temperature of 500 ± 2 °C and the composition $(\text{SnAs})_{0.70}\text{Sb}_{0.30}$. It intersects the section SnAs–

SnSb at the temperature of 408 ± 2 °C and the composition $(\text{SnAs})_{0.10}(\text{SnSb})_{0.90}$.

The line starting at U_1 (Fig. 4) separates the fields of primary crystallization of phases (SnAs) and (SnSb). The eutectic process $L \leftrightarrow (\text{SnAs})+(\text{SnSb})$ occurs along this line. This process should end at a four-phase equilibrium point. But in order to determine the character of this equilibrium we need to analyse the polythermal sections SnAs– Sn_4Sb_3 and Sn_4As_3 – Sn_4Sb_3 .

Assuming that a continuous solid solution is formed between Sn_4As_3 and Sn_4Sb_3 (which is quite probable, since they have the same crystalline structure and similar lattice parameters), we can suggest that the second four-phase equilibrium

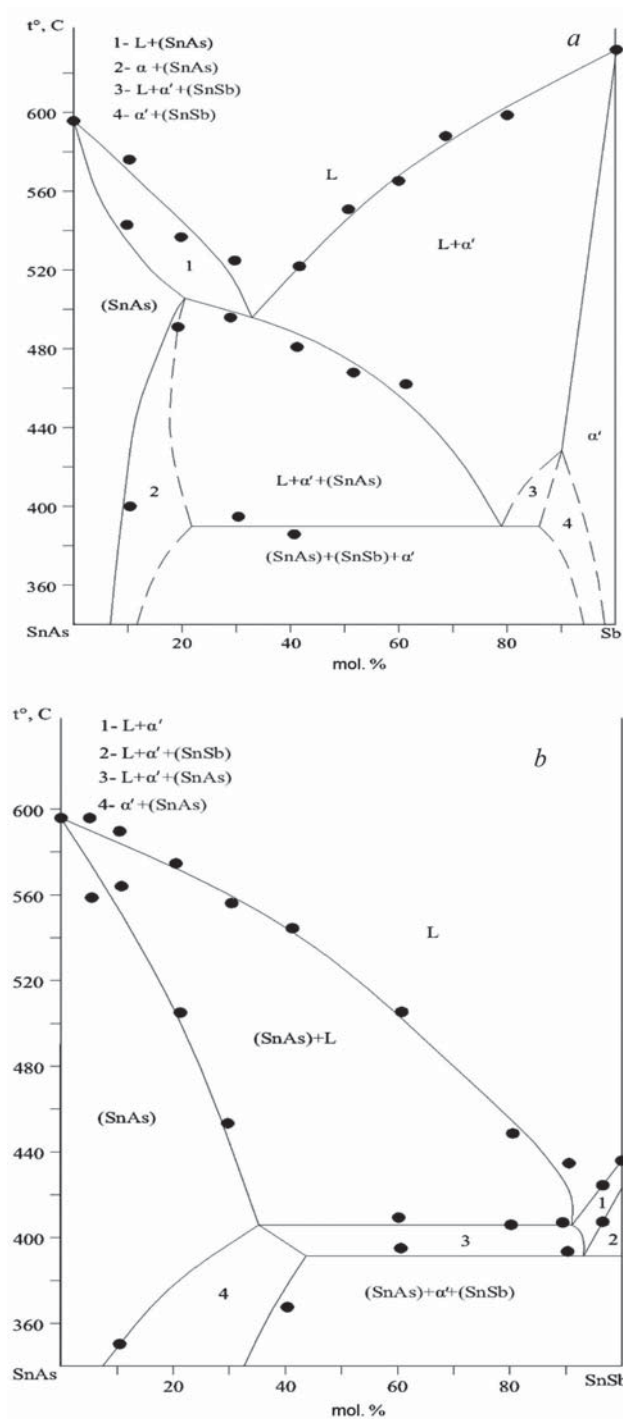


Fig. 5. T - x diagrams of the polythermal sections SnAs – Sb (a) and SnAs – SnSb (b)

point U_2 corresponds to the peritectic process $L + (\text{SnAs}) \leftrightarrow (\text{Sn}_4\text{As}_3)_{1-x}(\text{Sn}_4\text{Sb}_3)_x + (\text{SnSb})$.

4. Conclusions

The analysis of polythermal sections SnAs–Sb and SnAs–SnSb by X-ray phase analysis demonstrated that all the alloys include three phases, specifically solid solutions based on

SnAs and SnSb, and a solid solution of tin in phase $\text{As}_{1-x}\text{Sb}_x$ (α'). The concentration range of the solid solution based on tin monoarsenide along the section SnAs–Sb at room temperature is below 10 mol%; the solid phase solubility along the section SnAs–SnSb is below 5 mol% on both sides. Using the results of the differential thermal analysis and the XRD data T - x diagrams of polythermal sections SnAs–Sb and SnAs–SnSb were constructed. It was determined that at a temperature of 393 ± 2 °C the invariant peritectic equilibrium $L + \alpha' \leftrightarrow (\text{SnAs}) + (\text{SnSb})$ is present in the ternary system Sn–As–Sb. To construct a complete scheme of phase equilibria in the ternary system, further investigation of the SnAs– Sn_4Sb_3 and Sn_4As_3 – Sn_4Sb_3 sections is necessary.

Acknowledgements

The X-ray phase analysis was carried out using the equipment of the Centre for the Collective Use of Scientific Equipment of Voronezh State University.

Conflict of interests

The authors declare that they have no known competing financial interests or personal relationships that could have influenced the work reported in this paper.

References

- Hu Y., Lu Y. 2019 Nobel Prize for the Li-ion batteries and new opportunities and challenges in Na-ion batteries. *ACS Energy Letters*. 2019;4(11): 2689–2690. DOI: <https://doi.org/10.1021/acsenerylett.9b02190>
- Song K., Liu C., Mi L., Chou S., Chen W., Shen C. Recent progress on the alloy-based anode for sodium-ion batteries and potassium-ion batteries. *Small*. 2019;334: 1903194. DOI: <https://doi.org/10.1002/smll.201903194>
- Kulova T. L., Skundin A. M.. From lithium-ion to sodium-ion battery. *Russian Chemical Bulletin*. 2017;66(8): 1329–1335. DOI: [10.1007/s11172-017-1896-3](https://doi.org/10.1007/s11172-017-1896-3)
- Jing W. T., Yang C. C., Jiang Q. Recent progress on metallic Sn- and Sb-based anodes for sodium-ion batteries. *Journal of Materials Chemistry A*. 2020; Advance Article. DOI: <https://doi.org/10.1039/C9TA11782B>
- Kamali A. R., Fray D. J. Tin-based materials as advanced anode materials for lithium ion batteries: a review. *Reviews on Advanced Material Science*. 2011;27: 14–24. Available at: <http://194.226.210.10/e-journals/RAMS/no12711/kamali.pdf>

6. Wachtler M., Winter M., Besenhard J.O. Anodic materials for rechargeable Li-batteries. *Journal of Power Sources*. 2002;105: 151–160. DOI: [https://doi.org/10.1016/S0378-7753\(01\)00934-X](https://doi.org/10.1016/S0378-7753(01)00934-X)
7. Wachtler M., Besenhard J. O., Winter M. Tin and tin-based intermetallics as new anode materials for lithium-ion cells. *Journal of Power Sources*. 2001;94: 189–193. DOI: [https://doi.org/10.1016/S0378-7753\(00\)00585-1](https://doi.org/10.1016/S0378-7753(00)00585-1)
8. Xie H., Tan X., Lubner E. J., Olsen B. C., Kalisvaart W. P., Jungjohann K. L., Mitlin D., Buriak J. M. β -SnSb for sodium ion battery anodes: phase transformations responsible for enhanced cycling stability revealed by in situ TEM. *ACS Energy Letters*. 2018;3(7): 1670–1676. DOI: <https://doi.org/10.1021/acscenergylett.8b00762>
9. Li H., Wang Q., Shi L., Chen L., Huang X. Nanosized SnSb Alloy Pinning on hard non-graphitic carbon spherules as anode materials for a Li-ion battery. *Chemistry of Materials*. 2002;14(1): 103–108. DOI: <https://doi.org/10.1021/cm010195p>
10. Huang B., Pan Z., Su X., An L. Tin-based materials as versatile anodes for alkali (earth)-ion batteries. *Journal of Power Sources*. 2018;395: 41–59. DOI: <https://doi.org/10.1016/j.jpowsour.2018.05.063>
11. Zhang W., Pang W., Sencadas V., Guo Z. Understanding high-energy-density Sn_4P_3 anodes for potassium-ion batteries. *Joule*. 2018;2(8): 1534–1547. DOI: <https://doi.org/10.1016/j.joule.2018.04.022>
12. Jung S. C., Choi J., Han Y. The origin of excellent rate and cycle performance of Sn_4P_3 binary electrodes for sodium-ion batteries. *Journal of Materials Chemistry A*. 2018;6(4): 1772–1779. DOI: <https://doi.org/10.1039/C7TA07310K>
13. Domi Y., Usui H., Nakabayashi E., Yamamoto T., Nohira T., Hiroki Sakaguchi H. Potassiation and depotassiation Properties of Sn_4P_3 electrode in an ionic-liquid electrolyte. *Electrochemistry*. 2019;87(6): 333–335. DOI: <https://doi.org/10.5796/electrochemistry.19-00052>
14. Saddique J., Zhang X., Wu T., Su H., Liu S., Zhang D., Zhang Y., Yu H. Sn_4P_3 -induced crystalline/amorphous composite structures for enhanced sodium-ion battery anodes. *Journal of Materials Science & Technology*. 2019. In Press. DOI: <https://doi.org/10.1016/j.jmst.2019.05.032>
15. Zhang J., Wang W., Li B. Effect of particle size on the sodium storage performance of Sn_4P_3 . *Journal of Alloys and Compounds*. 2019;771: 204–208. DOI: <https://doi.org/10.1016/j.jallcom.2018.08.271>
16. Lan D., Li Q. $\text{Sn}_4\text{P}_3/\text{SbSn}$ nanocomposites for anode application in sodium-ion batteries. *ChemElectroChem*. 2018;5(17): 2383–2386. DOI: <https://doi.org/10.1002/celec.201800639>
17. Lee K. Synthesis and characterization of tetrel pnictides and compounds in the lithium-tetrel-arsenic system. *Dissertation*. University of California, Davis; 2016. 136 p. Available at: <https://search.proquest.com/openview/6c5577b9817fa2c2864fdeda33e2acfb/1?pq-origsite=gscholar&cbl=18750&diss=y>
18. Usui H., Domi Y., Yamagami R., Fujiwara K., Nishida H., Sakaguchi H. Sodiation–desodiation reactions of various binary phosphides as novel anode materials of Na-ion battery. *ACS Applied Energy Materials*. 2018;1(2): 306–311. DOI: <https://doi.org/10.1021/acsaem.7b00241>
19. Liu S., Zhang H., Xu L., Ma L., Chen X. Solvothermal preparation of tin phosphide as a long-life anode for advanced lithium and sodium ion batteries. *Journal of Power Sources*. 2016;304: 346–353. DOI: <https://doi.org/10.1016/j.jpowsour.2015.11.056>
20. Liu J., Wang S., Kravchik K., Ibáñez M., Krumeich F., Widmer R., Nasidou D., Meyns M., Llorca J., Arbiol J., Kovalenko M. V., Cabot A. SnP nanocrystals as anode materials for Na-ion batteries. *Journal of Materials Chemistry A*. 2018;6(23): 10958–10966. DOI: <https://doi.org/10.1039/C8TA01492B>
21. Liu C., Yang X., Liu J., Ye X. Theoretical Prediction of Two-Dimensional SnP_3 as a Promising Anode Material for Na-Ion Batteries. *ACS Applied Energy Materials*. 2018;1(8): 3850–3859. DOI: <https://doi.org/10.1021/acsaem.8b00621>
22. Saddique J, Zhang X., Wu T, Wang X., Cheng X., Su H., Liu S., Zhang L., Li G., Zhang Y., Yu H. Enhanced Silicon Diphosphide-Carbon Composite Anode for Long-Cycle, High-efficient sodium ion batteries. *ACS Applied Energy Materials*. 2019;2(3): 2223–2229. DOI: <https://doi.org/10.1021/acsaem.8b02242>
23. Schmetterer C., Polt J., Flandorfer H. The phase equilibria in the Sb-Sn system. Part I: Literature review. *Journal of Alloys and Compounds*. 2017;728: 497–505. DOI: <https://doi.org/10.1016/j.jallcom.2017.08.215>
24. Schmetterer C., Polt J., Flandorfer H. The phase equilibria in the Sb-Sn system. Part II: Experimental results. *Journal of Alloys and Compounds*. 2018;743: 523–536. DOI: <https://doi.org/10.1016/j.jallcom.2017.11.367>
25. Kovnir K. A., Kolen'ko Yu. V., Baranov A. I., Neira I. S., Sobolev A. V., Yoshimura M., Presniakov I. A., Shevelkov A. V. A Sn_4As_3 revisited: Solvothermal synthesis and crystal and electronic structure. *Journal of Solid State Chemistry*. 2009;182(3): 630–639. DOI: <https://doi.org/10.1016/j.jssc.2008.12.007>
26. Kovnir K. A., Kolen'ko Yu. V., Ray S., Li J., Watanabe T., Itoh M., Yoshimura M., Shevelkov A. V. A facile high-yield solvothermal route to tin phosphide Sn_4P_3 . *Journal of Solid State Chemistry*. 2006;179(12): 3756–3762. DOI: <https://doi.org/10.1016/j.jssc.2006.08.012>
27. Semenova G. V., Goncharov E. G. *Tverdye rastvory v trojnyh sistemah s uchastiem jelementov pjatoj grupy [Solid solutions involving elements of the fifth group]*. Moscow: MFTI Publ.; 2000. 160 p. (in Russ.)

28. Woo K. E., Dolyniuk J., Kovnir K. Superseding van der Waals with electrostatic interactions: intercalation of Cs into the interlayer space of SiAs_2 . *Inorganic Chemistry*. 2019;58(8): 4997–5005. DOI: <https://doi.org/10.1021/acs.inorgchem.9b00017>

29. Semenova G. V., Kononova E. Yu., Sushkova T. P. Polythermal section Sn_4P_3 – Sn_4As_5 . *Russian Journal of Inorganic Chemistry*. 2013;58: 1242–1245. DOI: <https://doi.org/10.7868/S0044457X13090201>

30. Kononova E. Yu., Semenova G. V., Sinyova S. I., Sushkova T. P. Phase equilibria in the Sn–As–Ge and Sn–As–P systems. *Journal of Thermal Analysis and Calorimetry*. 2014;117(3): 1171–1177. DOI: <https://doi.org/10.1007/s10973-014-3883-3>

31. Sushkova T. P., Semenova G. V., Naumov A. V., Proskurina E. Yu. Solid solutions in the system Sn–As–P. *Vestnik VGU. Serija: Himija. Biologija. Farmacija = Proceedings of Voronezh State University. Series: Chemistry. Biology. Pharmacy*. 2017;3: 30–36. Available at: <http://www.vestnik.vsu.ru/pdf/chembio/2017/03/2017-03-05.pdf> (In Russ., abstract in Eng.)

32. Semenova G. V., Sushkova T. P., Zinchenko E. N., Yakunin S. V. Solubility of phosphorus in tin monoarsenide. *Kondensirovannye sredy i mezhfaznye granitsy = Condensed Matter and Interphases*. 2018;20(4): 644–649. DOI: <https://doi.org/10.17308/kcmf.2018.20/639>

33. Okamoto H., Subramanian P. R., Kacprzak L., Massalski T. B. *Binary Alloy Phase Diagrams, Second Edition*. Ohio: ASM International, Materials Park; 1990. 810 p.

34. Allen W. P., Perepezko J. H. Solidification of undercooled Sn–Sb peritectic alloys: Part 1. Microstructural evolution. *Metallurgical Transactions A*. 1991;22: 753–764. DOI: <https://doi.org/10.1007/BF02670298>

35. Gokcen N. A. The As–Sn (Tin–Arsenic) system. *Bulletin of alloy phase diagrams*. 1990;11(3): 271–278. DOI: <https://doi.org/10.1007/bf03029298>

36. Emsli Dzh. *Elementy*. Moscow: Mir Publ; 1993. 256 c. (in Russ.)

Information about the authors

Tatiana P. Sushkova, PhD in Chemistry, Associate Professor, Department of General and Inorganic Chemistry, Voronezh State University, Voronezh, Russian Federation; e-mail: sushtp@yandex.ru. ORCID iD: <https://orcid.org/0000-0003-1969-7082>.

Galina V. Semenova, DSc in Chemistry, Professor, Department of General and Inorganic Chemistry, Voronezh State University, Voronezh, Russian Federation; e-mail: semen157@chem.vsu.ru. ORCID iD: <https://orcid.org/0000-0003-3877-985X>.

Aleksandra V. Sheveljuhina, postgraduate student, Department of General and Inorganic Chemistry, Voronezh State University, Voronezh, Russian Federation; e-mail: alexandrashevelyuhina@yandex.ru. ORCID iD: <https://orcid.org/0000-0002-0146-315X>.

Sergey V. Kannykin, PhD in Physics and Mathematics, Associate Professor, Department of Materials Science and Nanosystems Technologies, Voronezh State University, Voronezh, Russian Federation; e-mail: svkannykin@gmail.com. ORCID iD: <https://orcid.org/0000-0001-8756-5722>.

Elena Yu. Proskurina, PhD in Chemistry, Assistant, Department of General and Inorganic Chemistry, Voronezh State University, Voronezh, Russian Federation; e-mail: helko7@yandex.ru. ORCID iD: <https://orcid.org/0000-0002-6149-1398>.

Alexey V. Nerushev, MSc student, Faculty of Chemistry, Voronezh State University, Voronezh, Russian Federation; e-mail: alex.nerushev@yandex.ru. ORCID iD: <https://orcid.org/0000-0001-6285-3058>.

All authors have read and approved the final manuscript.

Translated by Yulia Dymant.

Edited and proofread by Simon Cox.